Anal Bioanal Chem (2002) 373:519–525
DOI 10.1007/s00216-002-1316-9

SPECIAL ISSUE PAPER

Bryan G. Splawn · Fred E. Lytle

On-chip absorption measurements using an integrated waveguide

Received: 9 January 2002 / Revised: 10 January 2002 / Accepted: 12 April 2002 / Published online: 21 June 2002

Abstract Square hollow waveguides are used to integrate measurement of absorption with chip-based electrophoresis. The 50×50 μm liquid channel and 50×50 μm waveguide are etched as a negative pattern into a silicon master and replicated as a positive in poly-dimethylsiloxane (PDMS). The uniform refractive index of the chip prevents guiding by total internal reflection. Instead, light at 488 nm is guided by reflection at the air-PDMS interface. The waveguide has a 60% efficiency over a distance of 3.2 cm. Separation of fluorescein and the dye BODIPY is demonstrated. A detection limit (S/N=3) of 200 μM fluorescein is obtained using a 50 μm pathlength and a simple photocell detector.

Keywords Waveguides · Absorption detection · Capillary electrophoresis · Poly-dimethylsiloxane · Chip

Introduction

Most detection schemes for chip-based electrophoresis employ off-chip optics with external sources and detectors that are bulky for microscale analysis. If the necessary optical components could be integrated with the separations channels it might be possible to shrink the size of the entire analytical system. Several groups have reported hybrid integration that include detector and source either fabricated on the separations chip or bonded to the chip [1, 2]. Other groups have used waveguides fabricated on the separations chip to carry light to and from the detector [3]. A drawback to such schemes is the cost associated with production of these specialty devices.

Dedicated to Professor David M. Hercules on the occasion of his 70th birthday

B.G. Splawn · F.E. Lytle (✉)
Chemistry Department, 1393 Brown Laboratories,
Purdue University, West Lafayette, Indiana 47907-1393, USA
e-mail: flytle@purdue.edu

It is well known that inexpensive poly-dimethylsiloxane (PDMS) replica chips can be prepared from a silicon master. Unfortunately, PDMS is not amenable to the creation of waveguides based on total internal reflection because it has a homogeneous, low refractive index. Nor is it currently compatible with the creation of hybrid sources and detectors. Numerous groups have combined fiber optics with electrophoresis chips [4, 5]. This approach is compatible with plastic replicas but is characterized by difficult alignment of the fibers with the liquid channel. Of particular concern is light which misses the liquid channel and reaches the detector. Additionally, it is difficult to design a simple optical arrangement where fibers can conveniently monitor multiple channels of separation.

Because of the above limitations, hollow waveguides were investigated as to their ability to guide light to and from the liquid channel. Hollow waveguides were developed by Bell Laboratories just prior to the advent of high-quality fiber optics [6]. These devices have a guide with a refractive index lower than the cladding, and trap light by the high reflection associated with grazing incidence angles. For replica chips the guide will be air (n=1) and the cladding PDMS (n=1.43). Hollow waveguides have an intrinsic loss, which is inversely proportional to the cube of the waveguide size. Because of this, most reported applications utilize sizes ranging from several millimeters to hundreds of microns [7, 8, 9, 10]. The smallest size reported in the literature is a cylindrical waveguide with a 250 μm diameter and a loss of 0.2 dB cm^{-1}.

The present study explores the utility of 50×50 μm square hollow waveguides for measuring absorption across a 50×50 μm liquid channel in PDMS replica chips. Because these waveguides are smaller by a factor of 5 than any described in the literature, their performance was evaluated and shown to have a propagation loss of 0.48 dB cm^{-1}. Performance of the entire chip was also examined. It was found that gated injection, although highly reproducible, effectively dilutes the sample by a factor of 22 when measuring absorption transverse to the liquid channel. Calibration curves were shown to be linear from ~10^{-4} to ~10^{-2} M, with a detection limit of 200 μM. Finally, the

separation of fluorescein and BODIPY was demonstrated.

Materials and methods

Solutions. All glassware was cleaned with several rinses of methanol and ultra-pure water and dried in an oven at 70 °C. Ultrapure water was obtained from a Nanopure filtering system (Barnstead, Dubuque, Iowa, USA) at ~18 MΩ cm and used in preparing buffer solutions. A 4 mM buffer solution was made using sodium tetraborate (Sigma, St. Louis, Mo., USA), then adjusted to pH 9.2 using sodium hydroxide (Fisher, Itasca, Ill., USA). Standard solutions of disodium fluorescein (Sigma) and BODIPY (Molecular Probes, Eugene, Ore., USA) were prepared in the range 1×10^{-4}–1×10^{-2} M using sodium tetraborate buffer as the diluent.

Fabrication. Microfluidic channels and an integrated waveguide were designed using a drawing software package (AutoSketch 7.0, San Rafael, Calif., USA). The design was anisotropically etched as a negative pattern onto a silicon wafer and replicated as a positive in PDMS. The silicon masters were made at the Stanford Nanofabrication Facility using deep reactive ion etching.

PDMS replicas were fabricated in-house. The silicon master was cleaned with methanol and deionized water and coated with a 5% soap (Ajax) and water solution. The soap and water solution was used as a releasing agent between the PDMS/silicon interface. Embossing of liquid channels and waveguides was performed with a 10:1 mixture of dimethylsiloxane (Sylgard 184 silicone) and curing agent (Essex Brownell, Columbia City, Ind., USA). The PDMS mixture was degassed under vacuum, poured onto the silicon master and allowed to harden over a 4-day period at room temperature. Replicas were carefully peeled off the master and rinsed with ethanol and deionized water. Figure 1 is a scanning electron microscopy (SEM) image of a 50×50 μm waveguide cast in PDMS. The aspect ratio appears to be at least 100:1. The rounding at the top disappears when capped with a glass cover plate, not shown in the figure. In addition, the glass cover plate provided a flat and rigid foundation for the flexible plastic replicas. Liquid reservoirs were cut from hollow glass tubing (1 cm OD/0.7 cm ID) using a diamond saw and glued onto the glass plate using Loctite 363 UV activated epoxy (Ed Hoy's, Warrenville, Ill., USA). The glass cover plate and PDMS replica were sealed using a PDC-001 oxygen plasma oxidizer (Harrick, Ossining, N.Y., USA). An irreversible seal was obtained by oxidizing the surfaces and bringing the two structures into contact. In addition, oxidation of the surface and subsequent contact with basic solutions supports electroosmotic pumping towards the cathode for both negatively and positively charged species [11].

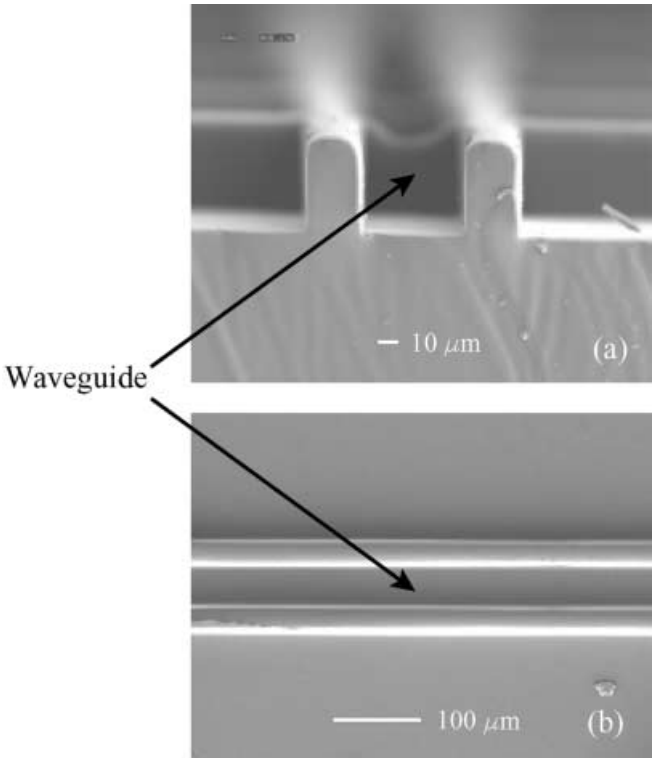

Fig. 1a, b Scanning electron microscopy (SEM) images of 50×50 μm waveguide replicated in poly-dimethylsiloxane (PDMS). Images represent the cross-section (**a**) and top views (**b**)

Instrumentation. A schematic of the instrumental setup is shown in Fig. 2. The light source was a continuous wave 488 nm argon ion laser (Melles Griot, Irvine, Calif, USA) operated at ~8 mW. The laser beam was focused via a plano-convex glass lens (Melles Griot) into the integrated hollow waveguide (right side of chip). Laser alignment into the waveguide was performed manually using multi-directional translation stages (Newport, Irvine, Calif, USA). Proper alignment was achieved when a square diffraction pattern of light exited the waveguide. Light was carried by the waveguide to the liquid channel, transmitted through a 25 μm window of PDMS, traveled across the liquid channel, then through a second window, and was collected by a second waveguide. Light exiting the second waveguide (left side of chip) was detected using a simple photocell (Edmund, Barrington, N.J., USA).

Two high-voltage power supplies (Gamma High Voltage, Ormond Beach, Fl.) were employed to initiate electrokinetic flow and inject samples using gated-injection [12]. The sample was loaded into reservoir A, and buffer into reservoir B. Electrophoretic separation involved a three-step process. Step one loaded channel A by setting E_A=1,000 V and E_B=1,600 V. With these potentials the sample moved from reservoir A toward reservoir C. By making $E_B>E_A$, no sample entered the separations channel. Step two injected a small amount of sample into the channels B and D by momentarily setting E_B=0 V. The length of time that B remained grounded determined the amount of sample injected. Step three returned E_B to 1,600 V. This established a potential gradient between the channel crossing and reservoir D, and caused electrophoretic migration and separation. Voltage control was maintained by LabVIEW 6i software (program written in-house) and a PCI 6035E data acquisition card (National Instruments, Austin, Tex., USA).

Results and discussion

Waveguide performance

There are five classes of loss that limit performance – alignment mismatches, diffraction across the liquid channel, insertion or mode-matching losses, reflective losses, and propagation losses. Simultaneous embossing of the waveguide and separations channel eliminates alignment losses such as those incurred when trying to incorporate external fiber optics. Diffraction losses depend upon the shape of the waveguide mode and the distance over which it must travel unguided, and are minimized by using the zero-order waveguide mode, which has a slowly varying transverse intensity. Insertion losses occur when the shape of the focused laser beam does not match the zero-order mode of the waveguide. Full mode-matching requires beam-shaping optics, while approximate mode-matching can be achieved by an appropriate choice of focusing lens.

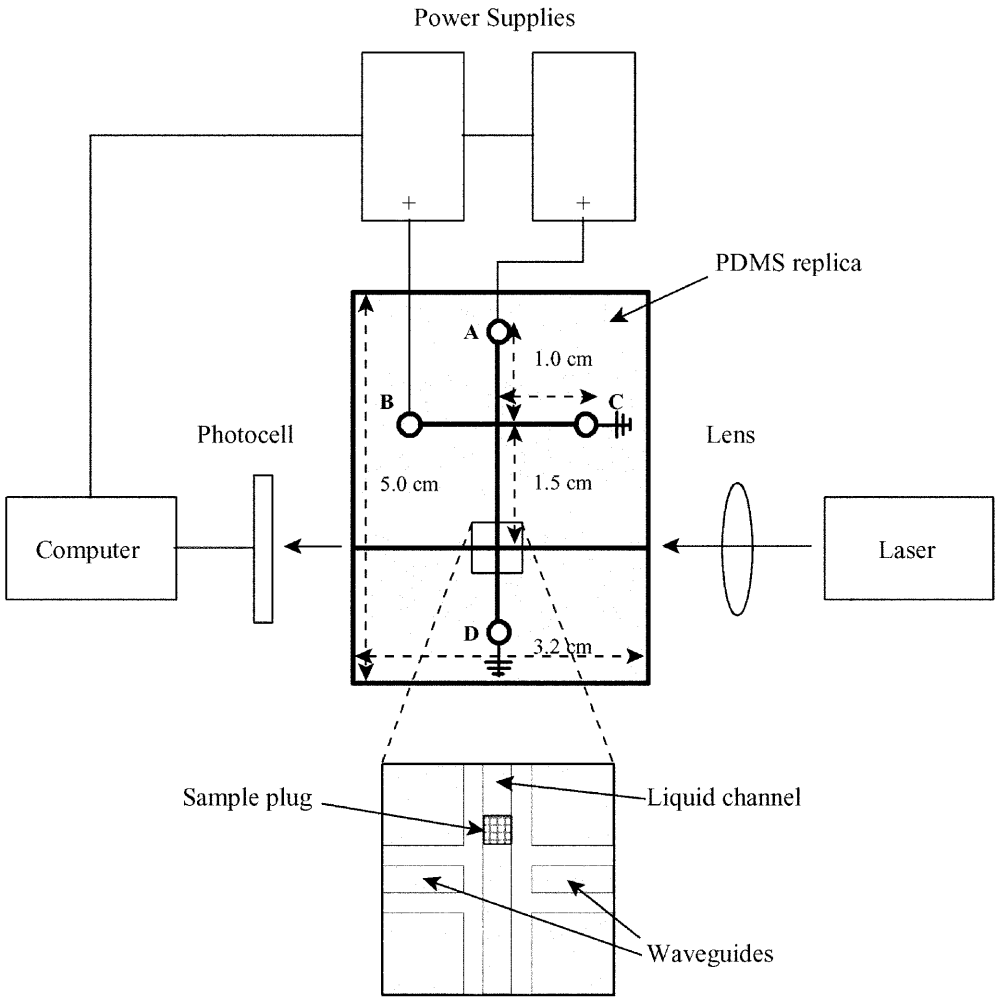

Fig. 2 Schematic of instrumental setup (*PDMS* replica is not drawn to scale). All liquid channels and waveguides are 50 μm wide and 50 μm deep. The detection surface area of the photocell is 1×1 mm in size. The entire system is automated with LabVIEW 6i

Reflective losses will occur with any optical scheme that involves refractive index boundaries, and are reduced by minimizing the number of surfaces through which the light needs to pass. Propagation losses are negligible when the refractive index of the waveguide is larger than that of the cladding. Hollow waveguides have a reverse refractive index ratio, and are thus intrinsically "lossy". Propagation performance of a hollow waveguide must then be gauged against the minimum loss predicted by theory and not the ideal value of 100% transmission.

For the chip used in this study the liquid channel is 50 μm wide and is separated from the incoming and outgoing waveguides by 25 μm thick windows. Thus the guided light has to "jump" unguided over a total distance of 100 μm. We have used numeric integration of the Fresnel-Kirchhoff diffraction integral [13] to determine that the zero-order mode of the 50×0 μm hollow waveguide has a diffraction loss of only 0.005 dB. This predicted loss is less than any other in the device, and has so far evaded measurement. The degree of mode-matching can be determined by a linear least-squares fit of the transverse intensity of the focused Gaussian beam to a sum of waveguide modes. This can be accomplished by a linear least squares procedure. The result predicts that best coupling (0.1 dB loss) to the zero-order mode will occur when the $1/e^2$ focal radius is equal to 0.35 times the waveguide width, i.e. 17.5 μm. Without adjusting the 1.4 mm radius of the beam entering the lens, the closest we could get to this value was 14 μm with a 120 mm focal length plano-convex lens. The corresponding insertion loss was 0.37 dB. With the present optical design, reflective losses occur at two air/PDMS boundaries (each 0.14 dB) and two PDMS/water boundaries (each 0.006 dB). This gives a total reflective loss of 0.29 dB.

The theoretical propagation loss of a cylindrical hollow waveguide was first developed by Marcatili and Schmeltzer [6], and extended to a variety of waveguides by Archambault et al. [14]. For a hollow square waveguide the propagation loss in dB cm^{-1} is given by the following:

$$\alpha_{dB} = 4.343(m+1)^2 \frac{2\lambda^2}{d^3} \frac{1}{2} \left(\frac{1}{\sqrt{n^2-1}} + \frac{n^2}{\sqrt{n^2-1}} \right) \quad (1)$$

, where the value 4.343 converts α from a base-e loss to decibels in base-10, m=0, 1, 2... is the mode number, λ is the wavelength in centimeters, d is the waveguide width in centimeters, and n is the refractive index of the waveguide wall. For m=0, $\lambda=488\times10^{-7}$ cm, $d=5.0\times10^{-3}$ cm, and n=1.43, the loss is predicted to be 0.25 dB cm^{-1}.

The measured overall waveguide transmission was 60% or a 2.22 dB loss. Subtraction of the diffraction, mode-matching, and reflective losses yields a propagation loss of 1.53 dB. The length of the waveguide was 3.2 cm for a 0.48 dB cm^{-1} loss. The factor of 1.76 between experiment and theory is not surprising, since a scanning electron micrograph of the waveguide shows a pattern of weak, horizontal striations on the two vertical side walls. These striations are due to reagent cycling in the Bosch etching process of the silicon master, and can be reduced by slower etching. Minimization of the insertion loss to 0.1 dB and the propagation loss to 0.25 dB cm^{-1} would lead to an overall loss of 1.17 dB or a 76% transmission, which is the best possible.

For a single channel of separation with absorption detection, the exact intensity of light reaching the detector is not overly important. It is simply necessary to have sufficient optical power to measure transmission with a high signal-to-noise ratio. Thus, the difference between the theoretical maximum of 76% and the observed 60% is of little practical concern. In contrast, simultaneous detection of multiple channels of separation will require integration of multiple waveguides with beam splitters and bends. Such configurations will benefit from waveguides with the lowest possible losses.

Gated injection

Figure 3 shows the measured peak shape as a function of injection time for a 3×10^{-3} M solution of fluorescein. For values of 250, 500 and 1000 ms, the full-width-at-half-maximum (FWHM) of the peak remains fairly constant at ~2.1 s. Beyond 1000 ms the FWHM increases in proportion to the injection time. The three longer injections all have a characteristic rise at early times that make the peaks asymmetric. The 500 ms injection time was chosen as the best compromise between peak shape (resolution) and maximum absorption (sensitivity). From Fig. 3 it can be determined that the electrophoretic mobility is 560 μm s^{-1}.

The peaks are much wider than predicted by injection time and migration rate. As an example, a Kirchhoff circuit analysis of the chip indicates that a 500 ms injection should create a 207 μm rectangle-shaped plug. The measured temporal width is 2.1 s, corresponding to 1,180 μm. Additionally, the expected trapezoidal shape is not observed at the detector. These discrepancies have been described in the literature for both gated and pinched injection as non-uniform electric field lines within the liquid channels [15, 16]. Additionally, Burke and Regnier have monitored a gated injection process nearly identical to ours with a video microscope [Burke BJ and Regnier FE, Purdue University (2001) unpublished work]. During the injection step when E_A=1,000 V and E_B=0 V, their data indicate that the electric field causes uniform transfer of sample from channel A into channel D (see Fig. 2 for labels) and non-uniform flow from channel A into channel B. With non-uniform flow, the sample is preferentially inserted along the channel edge connected to reservoir A. For short injection times, no sample reaches the opposite edge of channel B. For long injection times, channel B becomes loaded in the shape of an offset parabola with most of the sample along the edge connected to reservoir A. The extent of leakage into channel B is approximately the same whether E_B is grounded [17] or floated [15]. During the separation step when E_A=1,000 V and E_B=1,600 V, the flow from channel B into channel D preferentially occurs along the edge connecting those two reservoirs. For short injection times no sample enters channel D from channel B, and the higher flow along the connecting edge forces

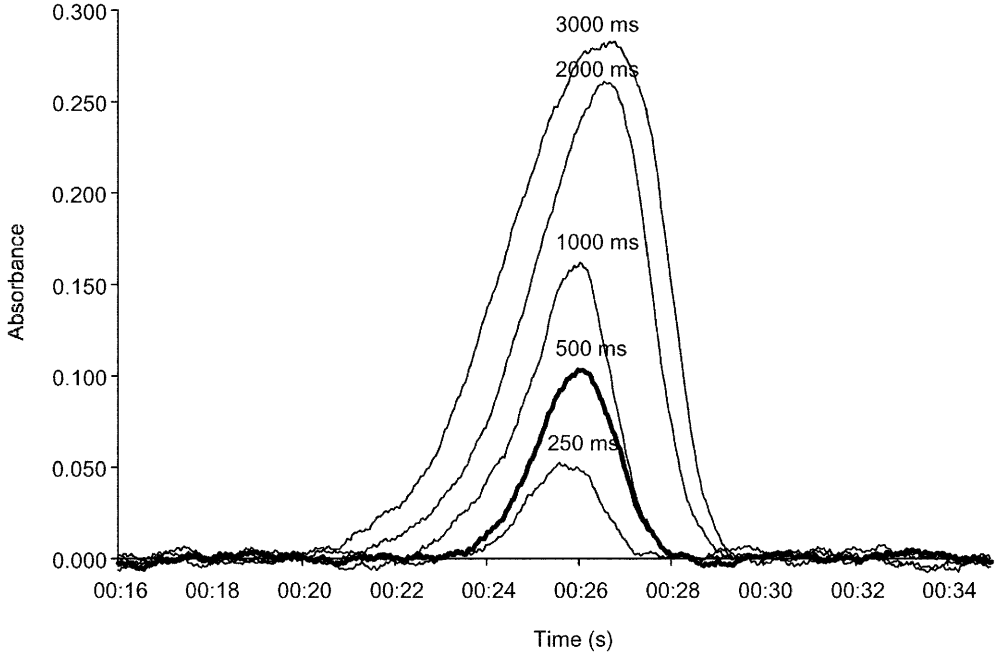

Fig. 3 Investigating peak shape relative to injection time using 3×10^{-3} M fluorescein in 4 mM sodium tetraborate buffer at pH 9.2

the sample plug into a diagonal configuration. With longer injection times the sample in channel B, closest to the BD connecting wall, is inserted into channel D. As injection time increases the back side of the sample plug slowly fills to form a triangular shape. These observations are qualitatively consistent with the shapes shown in Fig. 3.

Even with the unusual shape of the sample plug, gated 500 ms injection provided excellent peak-to-peak reproducibility. Figure 4 shows five injections of 5 mM disodium fluorescein made at 60 s intervals. The computed peak area had a 5% relative standard deviation. This uncertainty includes all sources of error including laser and detector noise. The slight increase in peak maximum with injection number is not generally observed.

With the two negatively charged compounds, disodium fluorescein and BODIPY, absorption returned to the baseline after each peak passed the detector. There was no evidence that sample was adsorbing to the capillary walls. This is in stark contrast to positively charged molecules such as acridine orange and rhodamine B. When sequentially injecting these samples, absorption did not quite return to the baseline. For a series of injections the baseline grew in steps as the compound was adsorbed onto the capillary walls. When injecting concentrated samples, posi-

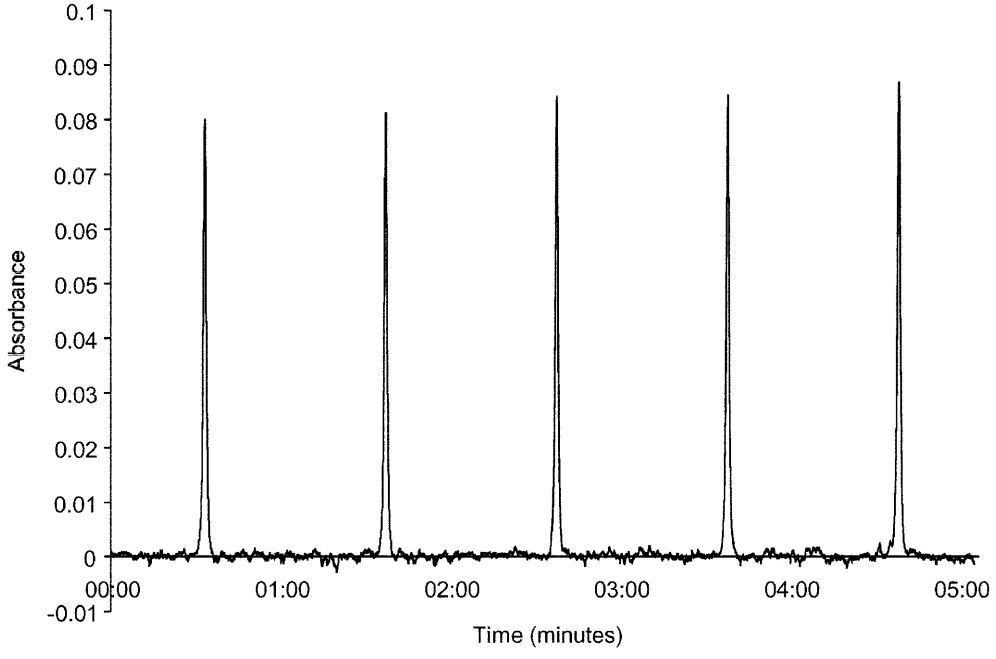

Fig. 4 On-chip reproducible injection and detection of 5×10^{-3} M fluorescein. Relative standard deviation is 5%

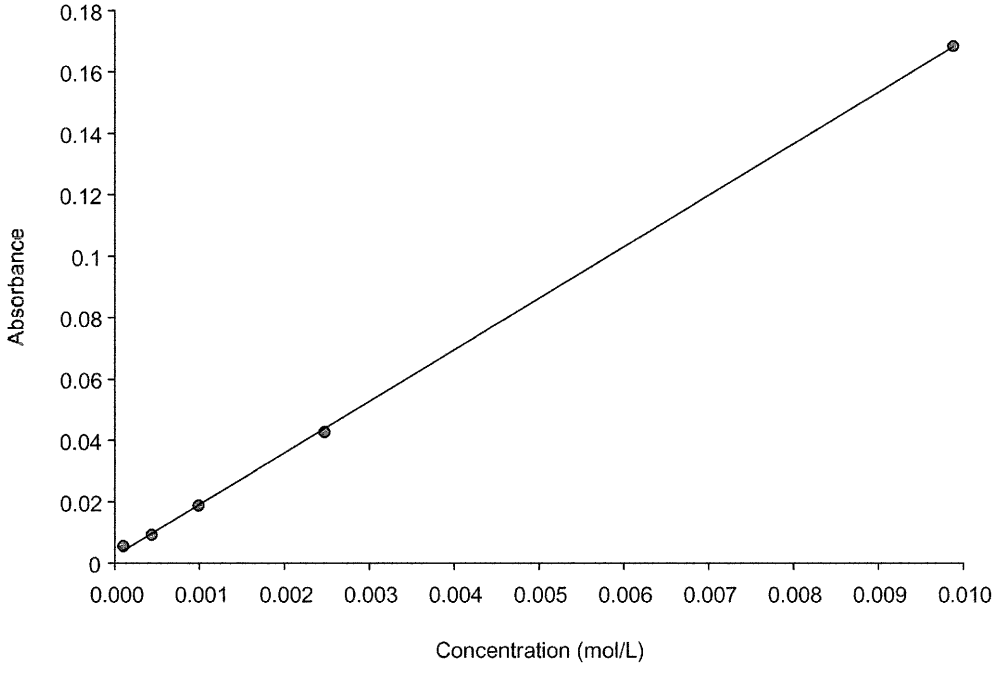

Fig. 5 Calibration curve of fluorescein. Concentrations range from 9.88×10^{-5} M to 9.88×10^{-3} M

tively charged dyes migrated into the PDMS, making the entire chip fluorescent.

Effective concentration

Various concentrations of disodium fluorescein in borate buffer were examined by placing them into reservoir A and setting E_A=1,000 V and E_B=0 V. This causes the sample to be continuously injected into channel D without dilution. These data were then used to compute a molar absorptivity of 73,000 L mol^{-1} cm^{-1}. This value agrees with an independent measurement made with a 10 μM solution and a 1 cm cell in a commercial spectrophotometer.

Because gated injection skews the sample plug, the observed absorption is about a factor of 22 lower than that expected on the basis of injected fluorescein molarity. As an example, the average peak height in Fig. 4 of 0.083 AU corresponds to an effective concentration of 0.23 mM. Note that the ratio of absorbance divided by the concentration is not constant between Fig. 3 and Fig. 4. The experiments were performed on two different chips. Small changes in injector behavior necessitate that each chip be individually calibrated.

Calibration plot

Transmission for a series of disodium fluorescein standards was measured on-chip. Light intensity from electrophoresis of pure buffer was defined as 100% T. This value and those measured during electrophoresis were converted into a plot of absorbance versus time. Calibration curve data are shown in Fig. 5 for injected concentrations ranging from 9.88×10^{-5} to 9.88×10^{-3} M. The linear dynamic range was over two orders of magnitude. A least-squares fit of the data yielded a slope of 16.78±0.14 L mol^{-1} and an intercept of 0.0024±0.0006 AU. The slope is a factor of 22 lower than the expected value of 365 L mol^{-1}.

Using the standard error of the fit (0.0012 AU), the detection limit (S/N=3) is computed as 200 μM for a 50 μm path length. When one takes into account path length differences, this value is only a factor of 12 worse than the value of 6 μM for a 140 μm path length reported by Liang et al. [5] and a factor of 5 worse than the value of ~3 μM for a 750 μm path length reported by Mogensen et al. [3]. The poorer performance can be accounted for by the fact that the present detection scheme is transverse to the direction of flow, while the other two are longitudinal. The sensitivity of transverse detection will decrease as the sample plug becomes skewed, whereas the sensitivity of longitudinal detection will be unaffected.

Separation of dyes

Figure 6 shows the electrophoretic separation of 3×10^{-3} M BODIPY and 3×10^{-3} M fluorescein. Baseline resolution was achieved using 4 mM sodium tetraborate/10% methanol solution at pH 9.2. Peaks were identified relative to the retention time of pure standards. Using an electrical field potential of 300 V cm^{-1}, the electrophoretic mobility for BODIPY was 530 μm s^{-1} and disodium fluorescein was 430 μm s^{-1}. Since methanol was added to the buffer solution to improve the separation, the mobility of fluorescein is slightly slower than in pure buffer (560 μm s^{-1}). This simple separation shows the applicability of integrating absorption detection with chip-based electrophoresis using hollow waveguides.

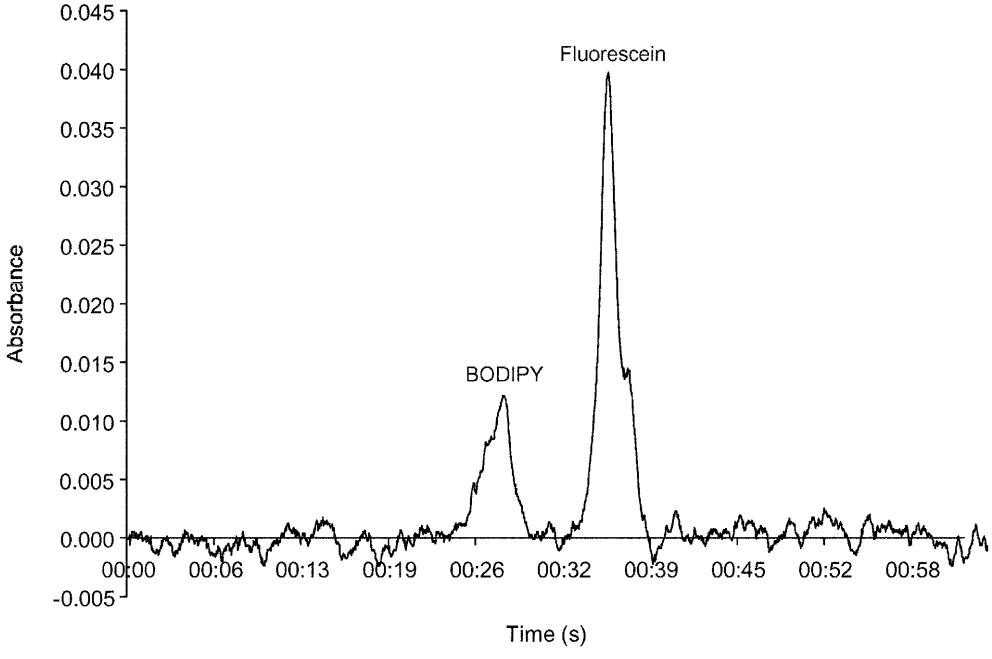

Fig. 6 Electrophoretic separation of 3×10^{-3} M BODIPY and 3×10^{-3} M fluorescein using 4 mM sodium tetraborate/10% methanol solution

Acknowledgements The authors gratefully acknowledge Dr. Mary Tang at the Stanford Nanofabrication Facility (Stanford, Calif., USA) for fabricating our silicon masters. We also thank Debra Sherman for imaging our PDMS replicas. The experimental advice from the research group of Dr. Fred E. Regnier is greatly appreciated. The Jonathan Amy Facility Center for Instrumentation (Purdue University, West Lafayette, Ind., USA) is also thanked for their helpful technical support. This work was supported by the National Institutes of Health (NIH Grant Number RR15231-02).

References

1. Burns MA, Johnson BN, Brahmasandra SN, Handique K, Webster JR, Krishnan M, Sammarco TS, Man PM, Jones D, Heldsinger D, Mastrangelo CH, Burke DT (1998) Science 282: 484–487
2. Kramer KD, Oh KW, Ahn CH, Boa JJ, Wehmeye KR (1998) Proc SPIE-Int Soc Opt Eng 3515:76–85
3. Mogensen KB, Petersen NJ, Hubner J, Kutter JP (2001) Electrophoresis 22:3930–3938
4. Manz A, Verpoorte E, Effenhauser CS, Burggraf N, Raymond DE, Widmer HM (1994) Fresenius J Anal Chem 348:567–571
5. Liang Z, Chiem N, Ocvirk G, Tang T, Fluri K, Harrison DJ (1996) Anal Chem 68:1040–1046
6. Marcatili EAJ, Schmeltzer RA (1964) Bell Sys Tech J 43:1783–1809
7. Matsuura Y, Abel T, Harrington JA (1995) Appl Opt 34:6842–6847
8. Kozodoy RL, Pagkalinawan AT, Harrington JA (1996) App Opt 35:1077–1082
9. Kozodoy RL, Micheels RH, Harrington JA (1996) Appl Opt 50:415–417
10. Roshan G, Harrington JA (2001) Proc SPIE-Int Soc Opt Eng 4204:230–237
11. Duffy DC, McDonald JC, Schueller OJA, Whitesides GM (1998) Anal Chem 70:4974–4984
12. Jacobson SC, Hergenroder R, Moore AW, Ramsey JM (1994) Anal Chem 66:4127–4132
13. Born M, Wolf E (1980) Principles of optics,6th edn. Cambridge University Press, Cambridge, UK
14. Archambault JL, Black RJ, Lacroix S, Bures J (1993) J Lightwave Technol 11:416
15. Jacobson SC, Ermakov SV, Ramsey JM (1999) Anal Chem 71: 3273–3276
16. Ermakov SV, Jacobson SC, Ramsey JM (2000) Anal Chem 72: 3512–3517
17. Burke BJ, Regnier FE (2001) Electrophoresis 22:3744–3751